Journal of Photochemistry and Photobiology A: Chemistry 201 (2009) 62–68

Contents lists available at ScienceDirect

Journal of Photochemistry and Photobiology A: Chemistry

journal homepage: www.elsevier.com/locate/jphotochem

Photocatalytic reduction of cadmium over $CuFeO_2$ synthesized by sol–gel

S. Bassaid[a], M. Chaib[a], S. Omeiri[b,c], A. Bouguelia[c], M. Trari[c,*]

[a] Laboratoire Chimie et Environnement, Faculté de Sciences, Université Ibn Khaldoun BP 78, 14000 Tiaret, Algeria
[b] Laboratoire de Stockage et de Valorisation des Energies Renouvelables, Faculté de Chimie BP 32, El alia 16111 Algiers, Algeria
[c] Centre de Recherche Scientifique et Technique en Analyse Physico-Chimiques BP 248, RP 16004 Algiers, Algeria

ARTICLE INFO

Article history:
Received 29 June 2008
Received in revised form
10 September 2008
Accepted 24 September 2008
Available online 15 October 2008

Keywords:
Photo-electrodeposition
Cadmium
Delafossite $CuFeO_2$
Water reduction

ABSTRACT

The Cd^{2+} photo-electrodeposition was successfully carried out in air-equilibrated aqueous $CuFeO_2$ suspension. The delafossite $CuFeO_2$ is *p*-type semiconductor characterized by a low optical gap, properly matched to the sun spectrum, and a long term chemical stability in neutral solution. It has been elaborated by the sol–gel technique where the specific surface area is increased via the surface/bulk ratio. The TG/DSC plots and IR spectra show that the solid phases are formed only at temperatures exceeding 400 and at 700 °C, the system is mixed phases. When fired at 950 °C under nitrogen flow, the delafossite has been identified ($CuO + CuFe_2O_4 \rightarrow CuFeO_2 + ½O_2$). All the XRD lines index in a hexagonal unit cell with the lattice constants $a = 284.2$ and $c = 169.4$ pm. The photocurrent onset potential (+0.35 V_{SCE}) is close to the flat band potential (+0.23 V_{SCE}) determined from the capacitance measurement. $CuFeO_2/Cd^{2+}$ solution is a self photo-driven system, the absorption of light promotes electrons into $CuFeO_2$–CB with a potential (−0.93 V_{SCE}) sufficient to reduce Cd^{2+}. This occurs because of the dark Cd^{2+} adsorption on the surface powder. The system was optimized with respect to the following physical parameters: pH 6.8, Cd^{2+} (100 ppm) and a mass concentration C_m (1 mg catalyst/ml solution). The hetero-system $CuFeO_2/TiO_2$ has been also reported for a comparative purpose. Prolonged irradiation (>50 min) was accompanied by a pronounced decrease in the rate of Cd-deposition owing to the competitive water reduction. Indeed, the generated bi-functional $CuFeO_2$/Cd particles account for the low over-potential of hydrogen and favour its evolution in aqueous solution.

© 2008 Elsevier B.V. All rights reserved.

1. Introduction

The metals (M) belonging to group II_B in the periodic table and their salts are well known for their high toxicity [1]. They are long lived and cannot be eliminated by biodegradation unlike organic pollutants [2]. The major sources of contamination come from industrial activities and the threshold concentration of metal ions poses a particular challenge for the water quality [3]. On the other hand, sun is a clean and inexhaustible source of energy and the conversion of sunlight to electrical and/or chemical energy is still the subject of intense investigations [4,5]. Some applications included photovoltaic devices [6], wet cells [7] and electrochemical solar convertors [8]. In the last decade, the photo-electrochemical (PEC) metal deposition became a major part of the environmental protection [9] and remains one of the most attracting targets for the research in the photodegradation of inorganic pollutants [10]. The semi conductor photoassisted catalysis has been widely employed [11]; the powder suspension does not require any sophisticated device and may be extended on large scales. The photo-electrochemistry is based on the excitation of a semiconductor by suitable light ($h\nu \geq E_g$), E_g being the forbidden band. The electrons in the conduction band (CB) undergo a cathodic metal and/or water reduction onto the surface catalyst. In presence of M^{2+}, the oxide is suitably biased to form a depletion layer leading to an efficient separation of photogenerated electron/hole (e^-/h^+) pairs. The reduction no longer holds if the M^{2+} adsorption is weak or the redox potential of the couple M^{2+}/M is too positive [12]. The PEC cadmium deposition is a major part of the protection of the ecosystem [13]. The ions Cd^{2+} are reduced to their elementary state on SC surface and can subsequently be extracted by physical and/or chemical methods [14]. A *p*-type electrode material should be chemically stable and must combine a small optical gap (E_g) and a positive flat band potential (V_{fb}). So, we emphasize the priority of searching novel materials for the PEC conversion and our investigations have been oriented towards oxides with new electronic structure. The delafossites $Cu^+B^{3+}O_2$ where B denotes a transition metal or a rare earth have received relatively little attention compared to the number of investigations using for example TiO_2 or WO_3. More recently, they begin to draw attention in the field of thin solid films [15], optoelectronic applications [16] and photo-

* Corresponding author. Tel.: +213 021 24 79 50; fax: +213 021 24 80 08.
E-mail address: Labosver@gmail.com (M. Trari).

1010-6030/$ – see front matter © 2008 Elsevier B.V. All rights reserved.
doi:10.1016/j.jphotochem.2008.09.015

catalysis [17]. The further advantage with these oxides is the high energetic position of CB giving the photoelectrons a strong reducing power, so attractive photocatalytic properties can be expected. To the best of our knowledge, no studies have been dealt with the recovery of metals over $CuBO_2$ much except our previous work [11]. Given the fact that there appears a direct gap transition of 1.3 eV, close the optimal value required for the sun light conversion and the foregoing features, $CuFeO_2$ is a promising photocatalyst for the reduction of heavy metals. In addition, the constituent elements Cu and Fe are by far the most interesting with regard to toxicity concern.

On the other hand, cadmium is known to be highly toxic and is released in large quantities in the aquatic environment without any control. It is commonly used in electroplating, protective coating and allowing agents in low melting alloys. Other uses are Ni–Cd batteries and neutron absorber in nuclear reactors (control rods) because of its large cross section for capture neutrons. The present work combines the solar energy to the environmental protection and is devoted to the reduction of Cd^{2+} over $CuFeO_2$ under visible light. The experiments were conducted under mild conditions close to those encountered in the aquatic natural media. Although not a general rule, the photoactivity is governed by the specific surface area and the PEC performance increases with decreasing the crystallite size [18]. Hence, it was attractive to synthesize the catalyst by the sol–gel technique [19]. The factors like the mass concentration, the pH of the solution, the complexation with EDTA have been optimized. The hetero-system $CuFeO_2/TiO_2$ is also reported for a comparative goal.

2. Experimental

All the chemical reagents were obtained from commercial sources and used as received without any further purification. The initial mixture, $Cu(NO_3)_2{\cdot}3H_2O$ (99%)/$Fe(NO_3)_3$,$9H_2O$ (98%) (0.025 M/0.025 M) was dissolved in 60 mL of ethylene glycol at room temperature for 2 hrs; the number between parentheses indicates the purity. The solution was heated under stirring at 70 °C for 6 h at reflux and the viscous solution was dried at 120 °C for 72 h. The powder was ground in an agate mortar and fired between 300 and 950 °C. The products have been characterized by X-ray diffraction (XRD) using Cu Kα radiation (λ = 0.154178 nm); the data were collected for 10 s. at each 0.02° step over a 2θ range (10–100°). TiO_2 (P25, 70% anatase) 99.8% purity has a specific surface of ∼50 m^2/g. The thermal analysis (TG) was carried out in air with a Setaram thermobalance (type 92-12-TGA) and a heating rate of 10 °C min^{-1}. DSC measurements were performed with a Setaram-192 apparatus; the powder was sealed in an alumina pan and heated up to 500 °C (5 °C min^{-1}). The surface area of $CuFeO_2$ (treated at 950 °C) was determined by the BET method using nitrogen gas as the adsorbate at liquid nitrogen temperature on ASAP 2010 icromeritics apparatus. The Fourier transform infrared transmission spectra (FT-IR) were recorded over the range (400–4000 cm^{-1}) with a Bio Rad-IR spectrometer with a resolution of 4 cm^{-1}. The samples were thoroughly mixed with dried spectroscopic KBr in a proportion of 1/100 and compacted into pellets under a uniaxial pressure of 2 kbar. For PEC characterization, the powder was pelletized under 2.3 kbar into 13 mm diameters discs of ∼1 mm thickness and sintered at 1040 °C (compactness ∼90%), above the oxide melt peritectically. Contact with copper wires was made onto the backside of pellet by using silver paint. The working electrode (0.86 cm^2) was encapsulated in a glass tube and isolated by epoxy resin. A three electrode cell was used for the intensity potential $J(V)$ characteristics, it includes a Pt sheet electrode (Tacussel, 1 cm^2) and a saturated calomel electrode. The working electrode was illuminated by a 200 W halogen tungsten lamp through a flat window and the potentials were monitored by a Voltalab PGP201 potentiostat. The extra pure KOH (0.5 M) electrolyte was flushed with nitrogen and the experiments were performed at room temperature. The photocurrent–photovoltage ($I_{ph} - U_{ph}$) characteristic was plotted in the cell $CuFeO_2/Cd^{2+}$/Pt with external resistance boxes and two multimeters.

The Cd^{2+} solutions were made down to 20 ppm by dilution from $Cd(NO_3)_2$,$4H_2O$ (Acros Organics, 99%). The photocatalytic tests were carried out in water cooled double walled reactor whose top was sealed with a rubber septum to allow the removal of the sample. The solution was maintained in the dark and the light was turned on after a transition period (15 h) required for the Cd^{2+} adsorption. Nevertheless, the adsorption kinetic was followed by chrono-potentiometry by measuring the potential of the Cd electrode (Tacussel) in $Cd^{2+}/CuFeO_2$ suspension. The light source was a HPK 125W Philips mercury lamp, emitting in the wavelength range 250–600 nm, with a maximum emission at 360 nm. A circulating water Pyrex-glass tank cooler, placed between the lamp and the reactor, was used for removing the heating effect. The temperature was regulated at 20 ± 1 °C by a thermo stated bath. The pH was adjusted to ∼6–7 and the air equilibrated suspension was magnetically stirred under constant agitation. During the photocatalytic test, 5 mL of the solution was taken out at regular time intervals and Cd^{2+} was analyzed by atomic absorption (SAA type UNICAM 939/959, λ = 228.8 nm). Before analysis, the suspension was filtered on a 0.45 μm Whatman filter to eliminate the catalyst particles. The Cd^{2+} concentration was evaluated by interpolation from a calibration curve. Blank runs were carried without the catalyst and in the dark. For the quantum efficiency (η), the light intensity was measured by a radio meter (HD 9021, Delta OHM) without correction for solution absorbance. The Cd^{2+} reduction proceeds in competition with the water reduction; the procedure and apparatus for hydrogen evolution have been described elsewhere [17].

3. Results and discussion

3.1. Physical and photoelectrochemical properties

It is a known fact that the photocatalytic activity of oxides is dependent on the preparative conditions and the light conversion efficiency increases with increasing the surface to volume ratio of the catalyst. Generally, enhanced photoactivity is attributed to the decreasing of the crystallite size. In the last decade, the synthesis by the sol–gel method has gained notoriety in the solid state chemistry. $CuFeO_2$ has been synthesized by this technique where the temperature is relatively low compared to the solid state reactions. The method does not require any high cost precursors and produces ultra fine powder with nanodimensions and consequently large active surface. At 950 °C under nitrogen flow, the pattern reveals a homogeneous $CuFeO_2$ single phase with a dark brown colour. Fig. 1 shows combined TG/DTG plot of noncalcined sample (CFO-NT); the first weight loss (∼35%) occurs at ∼200 °C and is originating from the departure of organic matter (ethylene glycol and oxalate) and the removal of adsorbed water. The second one at ∼300 °C comes from the nitrates decomposition. The plots of samples heated between 300 and 700 °C confirm such results and show the formation of stable oxides belonging to the ternary system Cu–Fe–O, above which a second weight loss is observed and which corresponds to the reaction:

$$CuO + CuFe_2O_4 \rightarrow CuFeO_2 + ½O_2$$

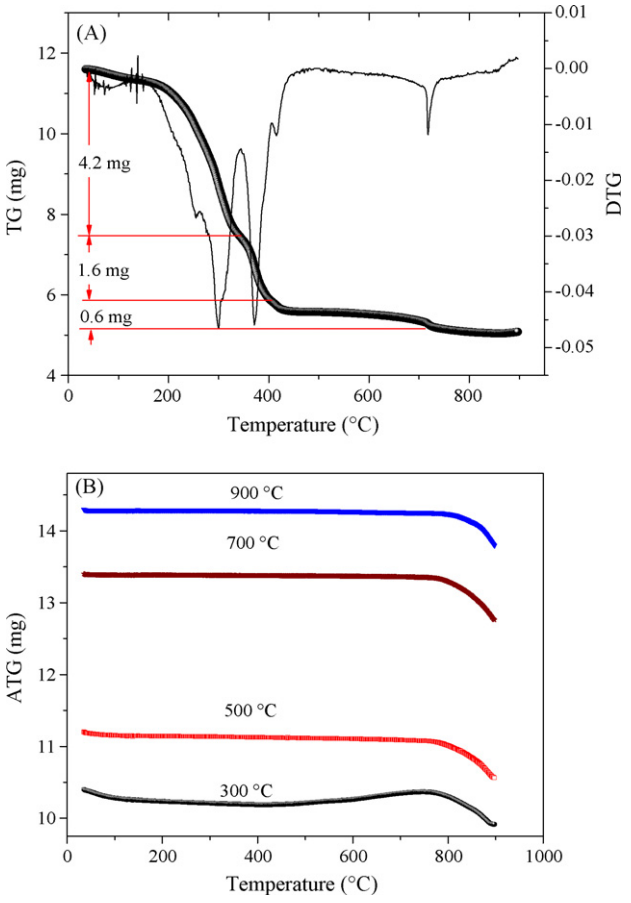

Fig. 1. TG plots of (A) noncalcined sample (CFO-NT); (B) samples calcined for 6 h at various temperatures.

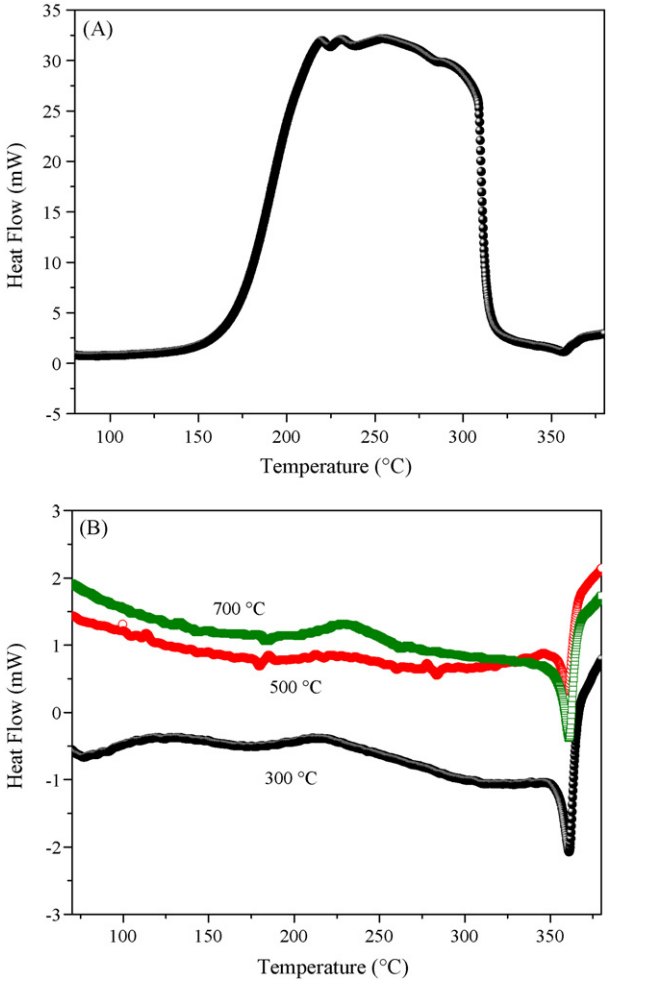

Fig. 2. DSC curves of (A) noncalcined sample (CFO-NT); (B) samples calcined at various temperatures.

Such transformations are corroborated by DSC plots (Fig. 2) where one notice a large exothermic (150–300 °C) corresponding to the presence of organic compounds above which the band completely disappears. Hence, one can conclude that the mineral phases are formed only beyond 400 °C.

The FT-IR spectrum of CFO-NT, depicted in Fig. 3, clearly shows an intense peak at 3400 cm^{-1}, characteristic of hydroxyl groups (O—H). The presence of ethylene glycol is confirmed by the peak at 915 cm^{-1}, attributed to the vibrations of CH_2 whereas the peak centred at ~1400 cm^{-1} is assigned to CO vibrations. At 300 °C the disappearance of bands 600–900 cm^{-1} and 1362 cm^{-1} characteristic of C–H groups and NO are due to the redox process between the ethylene glycol and nitrate. More interesting is the apparition of the peaks centred at 535 cm^{-1} assigned to Cu^{+} in linear coordination. To our knowledge, there is no mention in the literature concerning the IR absorption of monovalent copper in two fold coordination except the work reported on $CuAlO_2$ thin films [20]. These results indicate that the onset of conversion of amorphous gel to crystalline phases probably begin at 400 °C and was complete by 500 °C. At 700 °C in air, the XRD pattern (Fig. 4) shows only the reflections of the spinel $CuFe_2O_4$ along with those CuO and Fe_2O_3 and whose intensity decreases with increasing temperature of the calcination. After a final treatment at 950 °C, the XRD pattern exhibits only the peaks of $CuFeO_2$ which index in a hexagonal unit cell with the preferred orientation (123). The lattice constants $a = 28.42$ and $c = 169.46$ pm are in perfect agreement with those reported elsewhere [21]. The crystallite size L (50 nm) was estimated from the full width at half maximum (FWHM) (β) of the most intense peak (1 0 4) through the relation $\{L = 0.94\lambda/\beta\cos\theta\}$, θ being the diffraction angle. Assuming the crystallites to be spherical and nonporous, the specific surface area ($23 \pm 4\ m^2\ g^{-1}$) was deduced from the relation $\{=6/(Ld_{exp})\}$, d_{exp} (5.50 g cm^{-3}) being the experimental density. This value is slightly smaller than that obtained from BET ($28\ m^2\ g^{-1}$).

A band gap of 1.32 eV has been determined previously from the diffuse reflectance spectrum [11]. $CuFeO_2$ was chosen because of its long term chemical stability over the entire pH range. A corrosion rate in neutral solution, measured over six months of continuous operation through the titration of copper, was found to be only 1.32×10^{-2} μmol m^{-2} $year^{-1}$. It is now well established that oxygen inserts reversibly in the $CuBO_2$ layered lattice [22]. This gives the oxide *p*-type conductivity and allows PEC characterization. The cyclic $J(V)$ curve is illustrated in Fig. 5A. The dark current (J_d) is less than 1 mA cm^{-2} indicating a good electrochemical stability. The potential at which the J_d–V curve intercepts the potential-axis corresponds to the hydrogen evolution reaction (HER) and varies as a function of the oxygen partial pressure. In air equilibrated solution, the potential of the couple H_2O/H_2 (−0.65 V) is obtained by extrapolating a tangent line over the slope and prolonging it to zero current. The shape of the $J_{ph}(V)$ curve and the increase of the photocurrent (J_{ph}) in the negative-going potential (Fig. 5A, insert) confirm the *p*-type character of $CuFeO_2$ suggesting that the majority carriers are holes. The photocurrent onset potential ($V_{on} = 0.35$ V) is taken as the potential above which no photocurrent could be observed, and

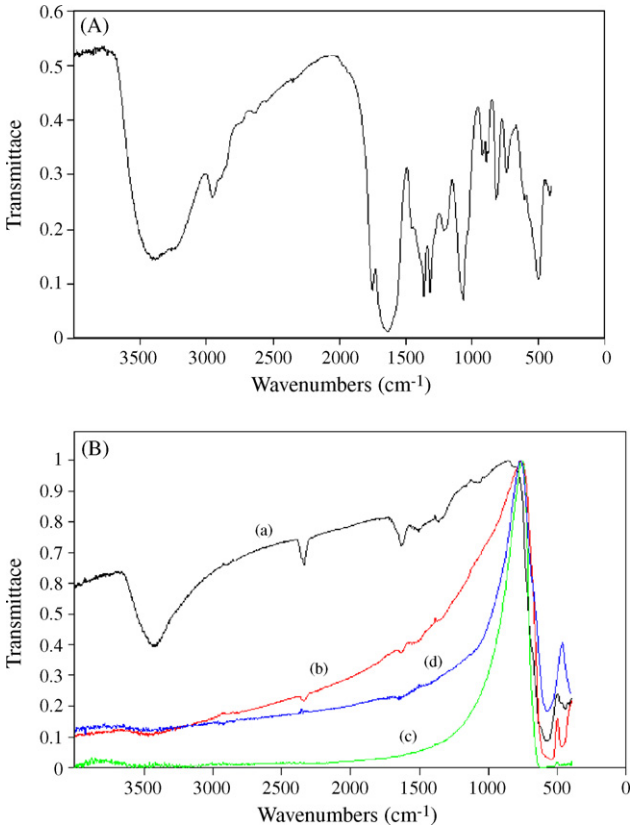

Fig. 3. The FTIR spectra of (A) noncalcined sample (CFO-NT); (B) calcined for 6 h at (a): 300 °C; (b): 500 °C; (c): 700 °C; (d): 950 °C.

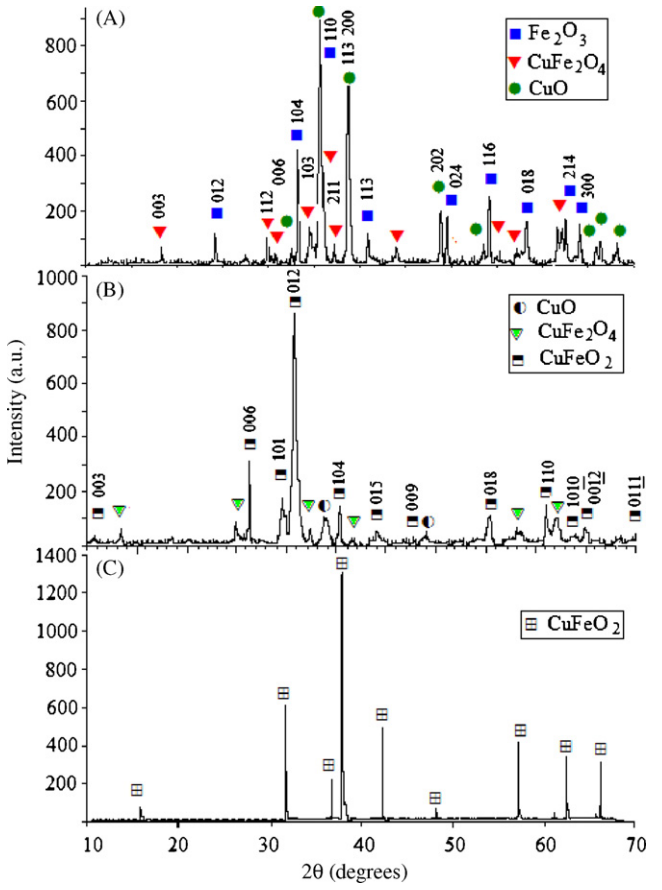

Fig. 4. Powder X-ray diffraction patterns of the sample: (A) heat treated at 700 °C for 6 h in air, (B) heat treated at 700 °C and 950 °C under nitrogen atmosphere for 12 h (C) after a second regrinding at 950 °C for 12 h.

can be assimilated to V_{fb} However, the potential V_{fb} is accurately determined from the capacitance measurement:

$$C^{-2} = \left(e\varepsilon\varepsilon_0 \mathrm{Na}\left\{V - V_{fb} - \frac{kT}{e}\right\}\right)$$

where the positive sign is for *n*-type and the negative sign for *p*-type conductivity, the symbols have their usual signification. The plot (C^{-2}–V) fits well with the experimental data with a good linearity (Fig. 5B), the potential V_{fb} (+0.23 V) is obtained from the intercept of the V-axis at $C^{-2} = 0$ and is close to V_{on} indicating a quasi absence of surface states within the gap region. The PEC properties of $CuFeO_2$ arise from CuO_2^{3-} entities, the crystal structure consists of close packed sheets of octahedral FeO_6 sharing common edges [23]. Two adjacent layers are linked to each other by bridged monovalent copper to $\{O{-}Cu{-}O\}^{3-}$ units parallel to the [0 0 1] direction. Both electronic bands are made up mainly of Cu-3*d* wave function; the lower filled t_{2g} orbital provides the valence band (VB) though being nonbonding is separated by ~2 eV from the lower lying O:2*p* whereas CB consists of empty hybridized $3dz^2/4$ s. This explains the chemical stability and gives a high energetic position of CB which provides photoelectrons able to reduce various metal ions to their elemental states [11].

A PEC cell is characterized by the J_{ph}–U_{ph} plot (Fig. 6A), recorded under variable load resistances. The fill factor (FF) defines the ideality of the system and is given by

$$\mathrm{FF} = \frac{J_m U_m}{U_{oc} I_{sc}}.$$

J_m and U_m can be evaluated by computing the product at various points along the plot and choosing that corresponding to the higher value which represents the useful maximal power. J_{sc} and V_{oc} are respectively the short circuit current and the open circuit voltage. The small FF (0.18) is due o the low hole mobility $CuFeO_2$ and the resistive nature of the pellet.

3.2. Photocatalysis

The PEC characterization permitted the establishment of the energy band diagram of the junction $CuFeO_2/Cd^{2+}$ solution (Fig. 6B). $CuFeO_2$–CB (−0.93 V), calculated from the relation ($V_{fb} + \Delta E - E_g$), is located below the redox potential E_{red} of Cd^{2+}/Cd couple. Accordingly, one can expect that Cd^{2+} might be thermodynamically photoreduced via CB process:

$$CuFeO_2 + h\nu \xrightarrow{h\nu \geq E_g} CuFeO_2(h^+_{VB} + e^-_{CB}) \quad (1)$$

$$Cd^{2+} + 2e^-_{CB} \rightarrow Cd \quad (2)$$

$$H_2O + 2e^- \rightarrow H_2 + 2OH^- \quad (3)$$

The efficiency of the metal deposition depends on the existence of the space charge region and the difference $|V_{fb} - E_{red}|$ measures the driving force of the junction. However, in nanoparticles, the band bending is small or inexistent and the charges separation occurs only by diffusion process. The electrons transfer takes place by injection mechanism and the net PEC process is governed exclusively by the electrons flow within the diffusion length of $CuFeO_2$ owing to their low mobility [24]. The whole PEC process takes place in a single crystallite with a compartmented reaction space of nanodimension. So, an additional condition to eventuate in photoreductions is that the free potential (U_f) of *p*-$CuFeO_2$ must be negative of V_{fb}. In our case, the potential U_f (−0.28 V) belongs to

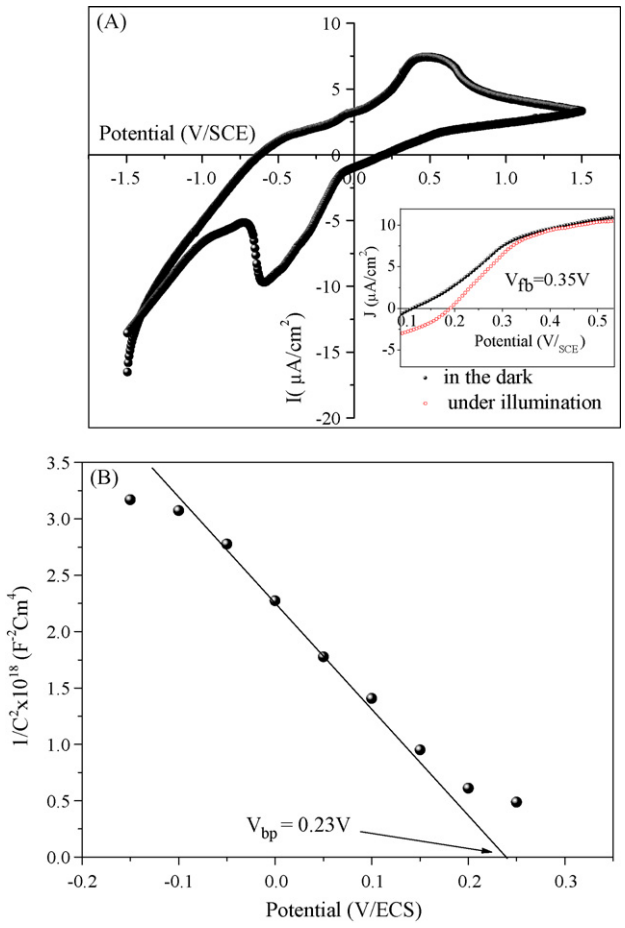

Fig. 5. (A) Cyclic $J(V)$ plot of $CuFeO_2$ in KOH (0.5 M) electrolyte. Insert: The $J(V)$ characteristics in the dark and under illumination. (B) The corresponding Mott–Schottky plot.

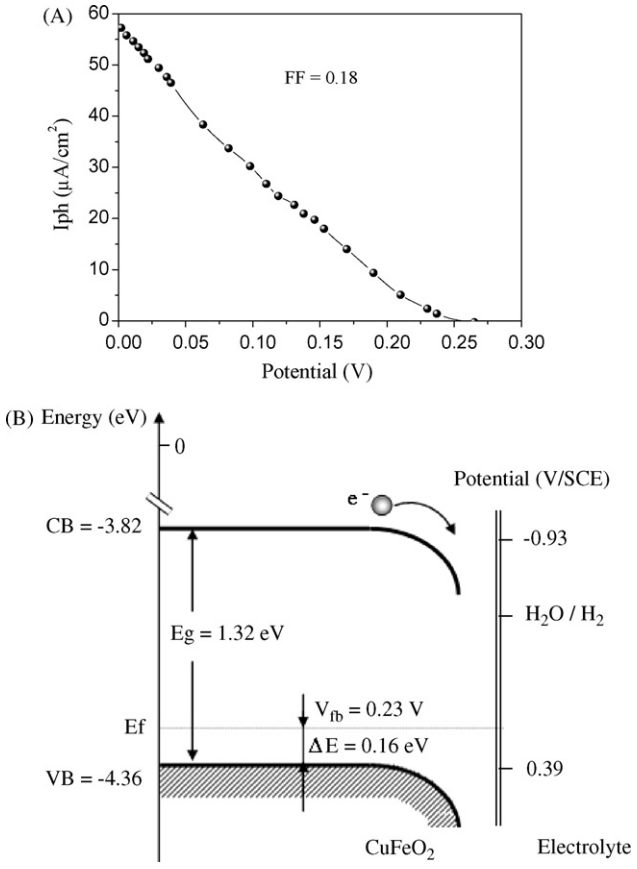

Fig. 6. (A) Photocurrent–photovoltage characteristic of the junction $CuFeO_2/Cd^{2+}$ solution. (B) The corresponding energy band diagram.

the immunity domain in the Cu–Fe–O phase diagram and the crystallite works like a micro PEC diode and is cathodically protected against the corrosion.

The main interest of this section is to investigate the effect of the physical parameters on the photoactivity. The pH of the solution has a direct influence on the metal deposition via the surface charge catalyst and in this way the pzzp. The physical adsorption is pH dependent and the equilibrium time depends on the nature of M^{2+} [12]. Let's recall that pzzp is the pH for which the net adsorbed charge on the surface is zero. With cadmium, the adsorption follows a cationic type law and is less accentuated at low pH. However, the experiments were conducted in air-equilibrated solution under mild conditions near to that observed in the aquatic media, Preliminary tests showed a dark Cd^{2+} adsorption which average 5% at pH 6.8. The best photo-electrodeposition occurs around this pH and a transition period is required before irradiation. So, the suspension was leaved in the dark overnight to ensure that the adsorption was $CuFeO_2$ equilibrated. However, the potential E_{red} (−0.59 V) and the dark adsorption time (~200 min) were determined by chronopotentiometery (Fig. 7); it corresponds to time where the potential becomes nearly constant (plateau region). Since both the levels Cd^{2+}/Cd and $CuFeO_2$–CB are pH insensitive, a pH change does theoretically not influence the PEC activity, and the variation can be easily understood in term of pzzp which is directly related to the adsorption affinity. The oxide has been prepared by the sol gel technique and the good performance of $CuFeO_2$ is attributed to Cd^{2+} adsorption which facilitates its reduction. Nevertheless, when the calcination temperature exceeds 900 °C, the crystallites can agglomerate in grains and decrease the specific surface area. This has been corroborated by the lack of XRD peak broadening and the relatively small active surface (28 $m^2\ g^{-1}$).

As expected, the amount of reduced cadmium is maximal at pH 6.8 (Fig. 8A) and decreases with decreasing pH. In acidic media (below pzzp, 7.6), the Cd^{2+} ions are repelled by the positive surface charge. The effect of physical parameters on the amounts of Cd^{2+}

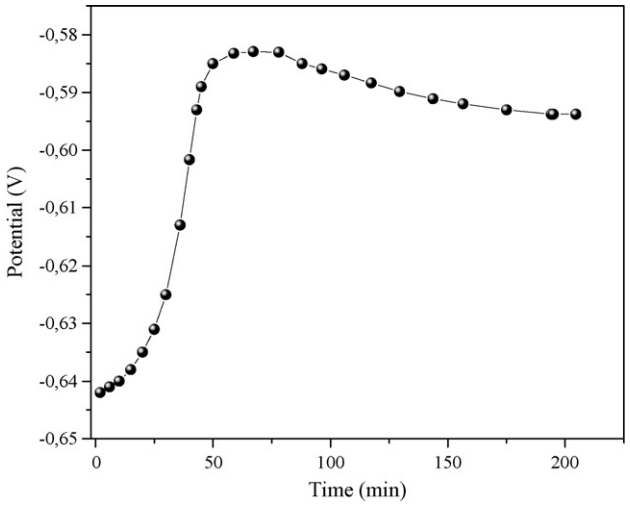

Fig. 7. Chronopotentiometric curve of the cadmium electrode in $CuFeO_2$ suspension immersed in Cd^{2+} solution.

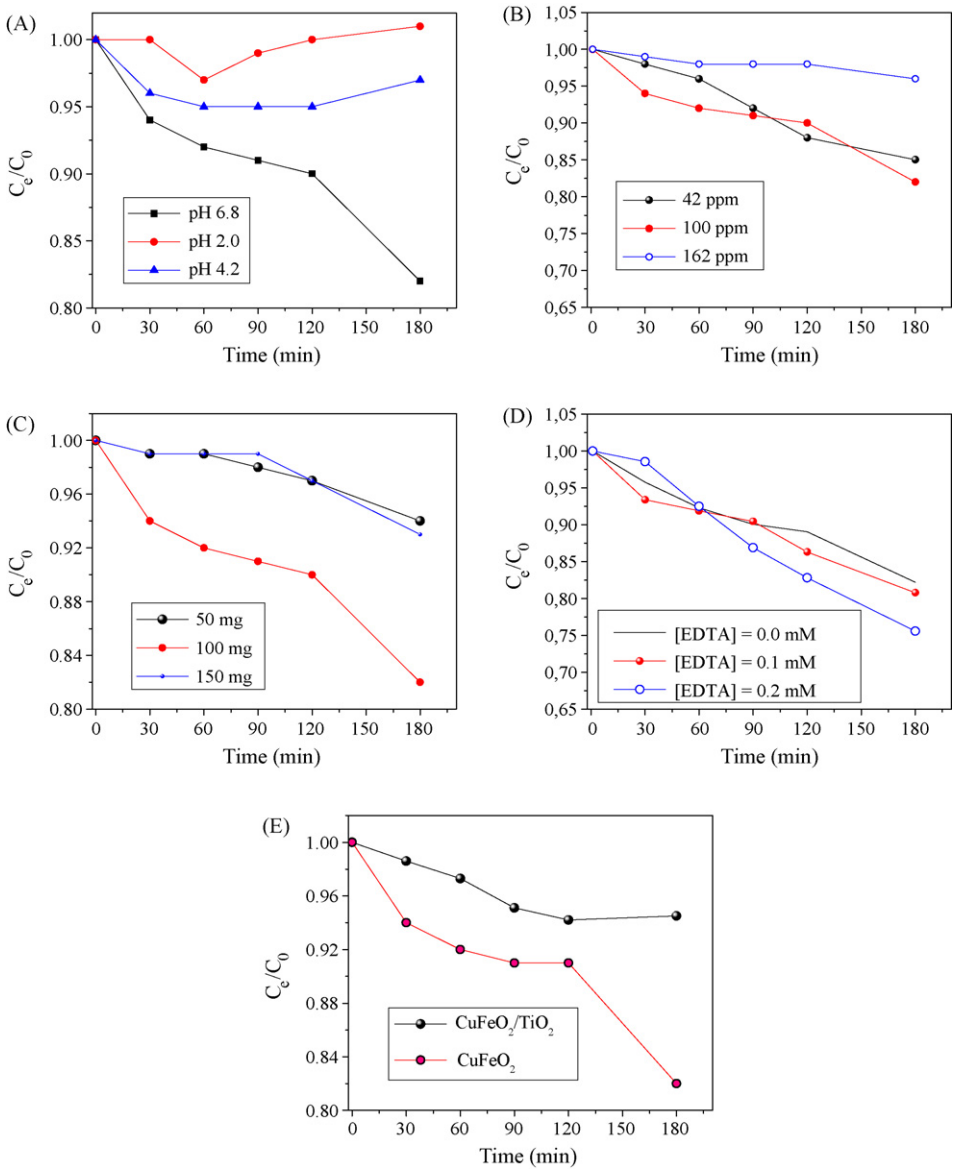

Fig. 8. Cadmium removal vs. time over $CuFeO_2$ suspension. The calcinations temperature of $CuFeO_2$ was 950 °C under nitrogen atmosphere: (A) at various pH. (B) at various catalyst mass. (C) with and without EDTA as complexant. (D) at various Cd^{2+} concentration. (E) of the hetero-junction.

removal (%) is summarized in Table 1 both in the dark and under illumination. The optimal concentration of Cd^{2+} was found to be 100 ppm (Fig. 8B).

The photocatalytic tests were carried out with various amounts of $CuFeO_2$ and the results, reported in Fig. 8C, give an optimal mass concentration C_m (mg catalyst per ml of solution). For smaller C_m, less active sites for the reduction process are available and the photoactivity increases in parallel with C_m. On the contrary, for higher C_m, all the sites are active and the light scattering of the incident flux, the shadowing effect of the grains catalyst as well as the metal clusters account for the decrease of the activity. Indeed, the incident light on the metal surface will be partially absorbed and converted to heat. The two opposing effects gave an optimal C_m value of 1 g L^{-1}. The complexation of cadmium inhibits the reduction process (Fig. 8D) thereby increasing the rate of the recombination of the (e^-/h^+) pairs and in this way decelerates the photo-reduction process; such procedure has been checked experimentally with EDTA as ligand. An optimal concentration of 0.2 mM has been obtained.

$CuFeO_2$ is found to be a good sensitizer [25] and the photoactivity is enhanced in the hetero-system (Fig. 8E) by the electron

Table 1
Effect of the physical parameters on the cadmium photo-electrodeposition illumination time 180 min.

	pH			Amount of catalyst (mg/100 mL)			Cd^{2+} concentration (ppm)		
	2	4.2	6.8	50	100	150	42	100	162
Dark adsorption (%)	0.0	3.98	4.48	6.5	17.4	4.48	8.54	6.51	7.59
Photoreduction (%)	0.0	2.72	17.6	5.97	17.6	7.11	31.5	17.6	4.07
Fixed parameters	$m_{catalysis}$ = 100 mg; [Cd^{2+}] = 100 ppm			pH = 6.8; [Cd^{2+}] = 100 ppm			$m_{catalysis}$ = 100 mg; pH 6.8		

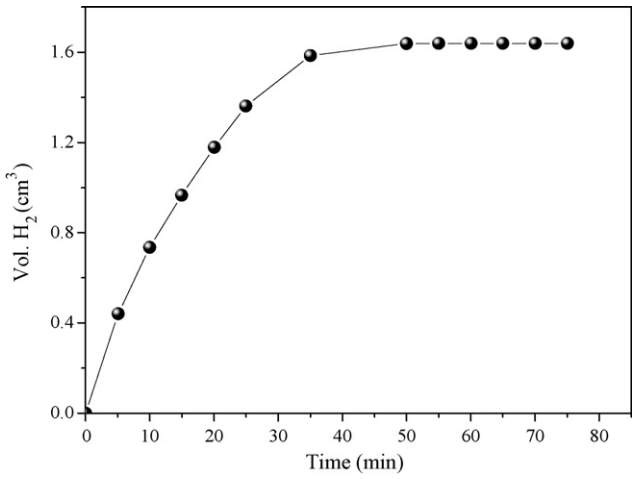

Fig. 9. Volume hydrogen produced as function of time of illumination of p-$CuFeO_2$ powder in neutral solution (pH ~ 7).

transfer from activated $CuFeO_2$–CB, working as an electron pump, to TiO_2–CB (−0.55 V) resulting in the reduction of Cd^{2+}. The quantum efficiency (η) of cadmium deposition is defined as

$$2\,\frac{\text{number of M deposited}}{\text{input number of photons}}$$

The factor 2 enters in the relation because the Cd^{2+} reduction is a two electrons event. Over time, the cadmium deposition drops after less than 1 h of continued irradiation. This tendency to saturation is due to the competitive reduction of water which takes place more easily than Cd deposition. This competition can be understood by the relation between the energy levels of $CuFeO_2$–CB, Cd^{2+}/Cd and H_2O/H_2 couple.

The potential of H_2O/H_2 usually varies with a change of pH: $-0.059\,V\,pH^{-1}$. The photoelectrons in $CuFeO_2$–CB can reduce either Cd^{2+} or water depending on pH. This is important for the solar energy conversion where a particular goal is desired. Hydrogen is clean an ideal of storing the solar energy. Metal modification of the surface SC has attracted much attention in the past [26]. The metals are suitable candidates for the water reduction as they are distinguished by low overvoltages. Indeed, the electrocrystallization of Cd onto p-$CuFeO_2$ can be regarded as an approach to improve the performance of hydrogen evolution. Once cadmium is deposited, the H_2 evolution proceeds in a nonhomogeneous fashion (Fig. 9); it can affect both the type of reaction and the interfacial charge transfer rate. The two materials $CuFeO_2$/Cd are coupled in a short circuited configuration via electrolytic solution. The potential of inter grains barrier is lowered and the electrons are channelled towards Cd catalytic sites where the over voltage is lower than that over oxides.

4. Conclusion

The present study focused on the photocatalytic assisted reduction of the environmentally harmful Cd^{2+}. We have successfully synthesized the delafossite $CuFeO_2$ by the sol gel route leading to an ultra fine powder and an increase of the surface/bulk ratio. The oxide is chemically stable and possesses a forbidden band, appropriately matched to the sun spectrum. These characteristics make it promising for the metal photo-electrodeposition. The oxygen insertion in the layered lattice yielded p conductivity and allowed the PEC characterization. The conduction band is more negative than the Cd^{2+}/Cd level giving spontaneous electrodeposition upon visible light. The catalytic tests were performed in air-equilibrated suspension at neutral pH to be close to the natural environment. The enhanced photoactivity is attributed to the increased specific surface area and consequently to good Cd^{2+} dark adsorption. The photoactivity has been optimized with respect to some physical parameters. In acidic media, the pH has a negative effect; the ions Cd^{2+} are pushed back by $CuFeO_2$ surface charged positively. The deposition occurred in less than one hour above which a tendency towards saturation was observed. The Cd photo-electrodeposition becomes disfavoured over the hydrogen evolution; the water discharge is therefore though the main reason for the regression in the Cd deposition. Light induced catalysis results in the deposition of ultra fine Cd particles onto $CuFeO_2$ where the interfacial charge transfer occurs easily through generated hetero-system.

Acknowledgments

This work was supported by Faculty of Chemistry (Algiers). We wish to express our gratitude to Dr. Y. Bessekhouad for helpful discussion.

References

[1] L.R. Skubal, N.K. Meshkov, T. Rajh, M. Thurnauer, J. Photochem. Photobiol. A: Chem. 148 (2002) 393.
[2] R. Brahimi, Y. Bessekhouad, A. Bouguelia, M. Trari, J. Photochem. Photobiol. A: Chem. 194 (2008) 173.
[3] D. Chen, A. Ray, Chem. Eng. Sci. 56 (2001) 1561.
[4] S. Saadi, A. Bouguelia, M. Trari, Sol. Energy 80 (2005) 272.
[5] M. Younsi, A. Aider, A. Bouguelia, M. Trari, Sol. Energy 78 (2005) 574.
[6] Al-Mohamed Ali, Appl. Energy 79 (2002) 345.
[7] A. Waheed, M. Badawy, J. Alloys Compds. (2007).
[8] Y.V. Kuminskii, G.Y. Kolbasov, Sol. Energy Mater. Sol. Cells 56 (1999) 93.
[9] M.I. Litter, Appl. Catal. B: Environ. 123 (1999) 89.
[10] L.B. Khalil, M.W. Raphael, W.E. Mourad, Appli. Catal. B: Environ. 36 (2002) 125.
[11] S. Omeiri, Y. Gabes, A. Bouguelia, M. Trari, J. Electroanal. Chem. 614 (2008) 31.
[12] W. Ketir, A. Bouguelia, M. Trari, J. Hazard. Mater. 158 (2008) 257.
[13] V.N.H. Nguyen, R. Amal, D. Beydoun, Chem. Eng. Sci. 58 (2003) 4429.
[14] T. Mishra, J. Hait, N. Aman, R.K. Jana, S. Chakravatry, J. Colloid. Interface Sci. 316 (2007) 80.
[15] M. Addamo, V. Augugliaro, A. Dipaola, E. Garcia-Lopez, V. Laddo, G. Marci, L. Palmicano, Thin Solid Films 516 (2008) 3802.
[16] A. Meagen, Marquardt, A. Nathan, Ashmore, David P. Cann, Thin Solid Films 496 (2006) 146.
[17] M. Younsi, S. Saadi, A. Bouguelia, A. Aider, M. Trari, Sol. Energy Mater. Sol. Cells 91 (2007) 1102.
[18] B. Marsen, B. Cole, E.L. Miller, Sol. Energy Mater. Sol. Cells 92 (2008) 1054.
[19] V. Ramaswamy, N.B. Jog tap, S. Vigayanand, D.S. Bhange, P.S. Awati, Mater. Res. Bull. 43 (2008) 1145.
[20] A.N. Banerrjee, S. Kundoo, K.K. Chattoopadhyay, Thin Solid Films (2003).
[21] J.P. Doumerc, A. Ammar, A. Winchainchai, M. Pouchard, P. Hagenmmmuller, J. Phys. Chem. Solids 48 (1986) 37–43.
[22] R.D. Shannon, D.B. Rogers, C.T. Prewitt, J. Inorg. Chem. 10 (1971) 713.
[23] M. Elazhari, A. Ammar, M. Elaatmani, M. Trari, J.P. Doumer, Eur. J. Solid State Inorg., Chem. 34 (1997) 503.
[24] M. Trari, J. Topfer, J.P. Doumerc, M. Pouchard, A. Ammar, P. Hagenmuller, J. Solid State Chem. 111 (1994) 104–110.
[25] A. Derbal, S. Omeiri, A. Bouguelia, M. Trari, Int. J. Hydrogen Energy 33 (2008) 4274.
[26] J. Akikusa, S.U.M. Khan, Int. J. Hydrogen Energy 27 (2002) 863–870.